Research Paper

Microarray Analysis of Long Non-Coding RNAs and Messenger RNAs in a Mouse Model of Oxygen-Induced Retinopathy

Lusi Zhang[1,2*], Xiaolin Fu[1,2,3*], Huilan Zeng[1,2], Jiang-Hui Wang[4,5], Yingqian Peng[1,2], Han Zhao[1,2], Jingling Zou[1,2], Liwei Zhang[1,2], Yun Li[1,2], Shigeo Yoshida[6], Yedi Zhou[1,2✉]

1. Department of Ophthalmology, The Second Xiangya Hospital, Central South University, Changsha, Hunan 410011, China
2. Hunan Clinical Research Center of Ophthalmic Disease, Changsha, Hunan 410011, China
3. Department of Ophthalmology, Hainan Western Central Hospital, Danzhou, Hainan 571799, China
4. Centre for Eye Research Australia, Royal Victorian Eye and Ear Hospital, East Melbourne, Victoria, Australia
5. Ophthalmology, Department of Surgery, University of Melbourne, East Melbourne, Victoria, Australia
6. Department of Ophthalmology, Kurume University School of Medicine, Kurume, Fukuoka 830-0011, Japan

* These authors contributed equally to this work.

✉ Corresponding author: Yedi Zhou, MD, PhD, Department of Ophthalmology, The Second Xiangya Hospital, Central South University, Changsha, Hunan 410011, China. Telephone: +86-731-85292175; E-mail: zhouyedi@csu.edu.cn

Abstract

Objective: Retinal neovascularization is a severe complication of many ocular diseases. To clarify the possible functions and therapeutic potential of long non-coding RNAs (lncRNAs) and messenger RNAs (mRNAs) in retinal neovascularization, we assessed their expression profile in a mouse model of oxygen-induced retinopathy (OIR).

Methods: Microarray analysis was performed to identify altered lncRNA and mRNA expressions between OIR and control mice. The microarray results were validated by qRT-PCR. Gene Ontology (GO) and Kyoto Encyclopedia of Genes and Genomes (KEGG) pathway analyses were conducted to determine biological functions and signaling pathways of the altered or interacted mRNAs. A coding-non-coding gene co-expression (CNC) network was constructed to identify the interaction of lncRNAs and mRNAs.

Results: We identified 198 up-regulated and 175 down-regulated lncRNAs (fold change≥2.0, P<0.05), respectively in OIR mice compared to control mice. We also identified 412 up-regulated and 127 down-regulated mRNAs (fold change≥2.0, P<0.05), respectively in OIR mice compared to control mice. GO and KEGG analyses suggested that altered mRNAs were enriched in immune system process, exopeptidase activity, ECM-receptor interaction and protein digestion and absorption. Four validated lncRNAs (ENSMUST00000165968, ENSMUST00000153785, ENSMUST00000134409, and ENSMUST00000154285) and the nearby coding gene pairs were analyzed. A CNC network profile based on those validated altered lncRNAs as well as 410 interacted mRNAs was composed of 509 connections. Moreover, the GO and KEGG analyses demonstrated that these interacted mRNAs mainly enriched in blood vessel development, angiogenesis, cell adhesion molecules and leukocyte transendothelial migration pathways.

Conclusion: Our data highlight the utility of altered lncRNA and mRNA profiling in understanding the pathogenesis of ischemia-induced retinal neovascularization and further suggest that therapeutic potential of altered lncRNA for retinal neovascularization.

Key words: lncRNA, mRNA, microarray, expression profile, oxygen-induced retinopathy, retinal neovascularization, angiogenesis

Introduction

Proliferative diabetic retinopathy (PDR), retinopathy of prematurity (ROP) and retinal vein occlusions are major causes of blindness worldwide, and retinal neovascularization is the key pathogenesis of these ocular diseases [1]. Although anti-vascular endothelial growth factor (VEGF) therapies have been

applied in those retinal neovascular diseases [2], the effect and efficiency is not satisfied in some patients[3], and intravitreal injection of anti-VEGF agents may also lead to numerous systemic and local complications, such as tractional retinal detachment, endophthalmitis and acute elevation of blood pressure [2, 4]. Thus, identification of novel targets that play important roles in retinal neovascularization is urgently needed to treat patients who are not responsible for anti-VEGF therapy.

Long non-coding RNAs (lncRNAs) are more than 200 nucleotides long that function at chromatin organization [5], transcriptional and post-transcriptional regulation [6]. LncRNAs locate in the nucleus and/or cytoplasm, and are recognized to be expressed in a tissue-specific manner [7], indicating that lncRNAs may play crucial regulatory roles in a wide range of biological and pathological processes [8-12]. Moreover, studies have shown that dysregulation of lncRNAs is associated with several ocular diseases, such as diabetic retinopathy [13, 14], glaucoma [15], proliferative vitreoretinopathy [16] and retinoblastoma [17]. Moreover, targeting some important lncRNAs, such as MIAT [14] and MALAT1 [18], have been proved to ameliorate pathogenesis of diabetic microvascular complication. Oxygen-induced retinopathy (OIR) is a mouse model which widely used in investigating retinal neovascularization [19-21]. However, the expressions profile and functions of lncRNAs in retinal neovascularization still remain unclear in this model.

In this study, we performed microarray to profile the lncRNAs and mRNAs expression in a mouse model of OIR. Subsequently, we interrogated the putative functions of the altered lncRNA and mRNAs through the *in silico* analysis to reveal the underlying regulatory networks in retinal neovascularization. Our results provide a clue for understanding the potential mechanism of ocular pathological neovascularization on the lncRNA aspect.

Materials and Methods

Animals and ethics statement

C57BL/6J mice were purchased from Hunan SJA Laboratory Animal Co., Ltd. and were used in all experiments. All of the experimental procedures in the present study were approved by the Institutional Animal Care and Use Committee of Central South University, China. Animals were treated based on the ARVO Statement for the Use of Animals in Ophthalmic and Vision Research.

Oxygen-induced retinopathy mouse model

OIR mouse model was induced as previously described [19-21]. In brief, newborn pups were exposed to 75% oxygen at postnatal day 7 (P7), and were returned to room air 5 days later at P12. We used pups kept in room air continuously as the control group. Retinas were collected at P17 in both OIR and room air control mice.

Microarray analysis

We isolated total RNA from retinas by using Trizol RNA extraction kit (Invitrogen life technologies). Retinas from both eyes of a mouse were mixed as one sample. The quantification of RNA was assessed by Nano Drop ND-1000, and standard denaturing agarose gel electrophoresis was performed to evaluate RNA integrity. The expression profile of lncRNAs and mRNAs were detected by Arraystar Mouse LncRNA Microarray (V3.0, including 35923 lncRNA and 24881 mRNA transcripts). A total of 6 samples (3 OIR and 3 room air controls) were used for microarray analysis. The tissue preparations and microarray hybridization were performed by using the Agilent Gene Expression Hybridization Kit (Agilent Technology, USA). Acquired array images were analyzed by Feature Extraction software (Agilent Technologies, version 11.0.1.1).

Quantitative real-time reverse transcription polymerase chain reaction (qRT-PCR)

Total RNA of 500 ng was reverse-transcribed using RevertAid First Strand cDNA Synthesis Kit (Thermo Scientific, Waltham, MA, USA) and oligo (dT) primers. Quantitative PCR primer sequences are listed in Table 1. qRT-PCR was conducted on the Applied Biosystems® StepOneTM Plus Real-Time PCR System (Thermo Scientific, Waltham, MA, USA) using FastStart SYBR Green Master (Sigma, St. Louis, MO, USA). Relative quantification data were normalized to β-actin and analyzed by ΔΔCt method which has been previously described by Livak[22].

Gene Ontology (GO) analysis, Kyoto Encyclopedia of Genes and Genomes (KEGG) pathway analysis and lncRNAs/mRNAs co-expression network

To reveal putative biological changes in mRNA profile and the possible influence of these co-expressed genes and lncRNAs between OIR and control mice, GO analysis (http://www.geneontology.org) and KEGG pathway analysis (http://www.genome.jp/kegg/) were conducted on altered mRNAs, and the interacted mRNAs within the network.

This coding-non-coding gene co-expression (CNC) network was constructed from 4 validated lncRNAs, and the Pearson correlation coefficients (PCCs) ≥ 0.99 was chosen as the baseline of correlation analysis. Cytoscape V2.8.3 (The Cytoscape Consort-

ium, San Diego, CA, USA) was used to graphically represent the interaction.

Statistical Analyses

The statistical difference was assessed by *Student t*-test. Differentially expressed RNAs were identified by fold change (FC)≥2.0 and P＜0.05.

Results

Altered lncRNA and mRNA expression identified in mouse OIR retinas

To investigate the potential difference in retinal lncRNAs and mRNAs expression profile between OIR mice and room air controls, the microarray was performed to detect 35,923 lncRNAs and 24,881 mRNAs transcripts. Our microarray data analysis revealed that 198 and 175 lncRNAs were significantly upregulated and downregulated, respectively in OIR retinas compared to room air controls (FC ≥ 2.0, P<0.05) (Fig.1A, Supplementary Table 1). The top 20 most significantly altered (both upregulated and downregulated) lncRNAs are listed in Table 3-4. The hierarchical cluster of heat map (Fig. 1C) showed the top 20 significant upregulated and downregulated lncRNAs, and ENSMUST00000153785 and NR_037990 are up- and down-regulated lncRNA transcripts with the most significant changes. Moreover, the hierarchical cluster analysis in Fig. 1C suggested successfully classified lncRNAs expression profile among OIR mice and controls.

We also identified that 412 and 127 significantly increased and reduced mRNAs, respectively in OIRs compared to room air controls (fold change ≥ 2.0, P<0.05) (Fig.1B, Supplementary Table 2). The top 20 significantly altered (both upregulated and downregulated) lncRNAs are listed in Table 5-6. Among them, edn2 and fmo3 are the up- and downregulated genes with the most significant changes in OIR retinas. Meanwhile, the hierarchical cluster of heat map (Fig. 1D) also showed the classification of mRNAs expression profile in the P17 OIR retinas as well.

Validation of differential lncRNAs expression by qRT-PCR and nearby coding gene expression analyses

LncRNAs were selected for qRT-PCR validation from those which have their nearby associated coding genes, and the genomic position of the coding gene is within 300kb upstream or downstream of the altered lncRNA region. Four lncRNAs, ENSMUST00000165 968, ENSMUST00000153785, ENSMUST00000134409, and ENSMUST00000154285 were selected to validate the altered lncRNAs in microarray analysis by

qRT-PCR. The results showed that the expression of ENSMUST00000165968 and ENSMUST00000153785 was significantly increased to 11.60±3.25-fold and 46.16±13.39-fold in OIR mice (p=0.0173 and p=0.0151, respectively; Fig. 2). Likewise, ENSMUST00000134409 and ENSMUST00000154285 were significantly decreased to 0.24±0.024-fold and 0.30±0.093-fold in OIR mice (p<0.0001 and p=0.0336, respectively; Fig. 2). The qRT-PCR results were consistent with the microarray altered expression data in Table 2. These data suggested the reliability and reproducibility of the lncRNAs expression profile detected by microarray.

To explore the possible role of altered lncRNAs in local regulation of gene expression [23], we further analyze the nearby coding gene pairs (distance≤300 kb) based on the genomic information of the validated lncRNAs. We found that the expression level of the lncRNAs' nearby genes all increased significantly in OIR retina (Table 2). For example, serpina3 within upstream of ENSMUST00000165968 and FGF2 within the intronic antisense strand of ENSMUST000001537 85 were up-regulated in OIR retina compared to control, respectively. Moreover, COL4A2 within upstream of ENSMUST00000134409 and C1QA within downstream of ENSMUST00000154285 showed increased expression levels.

GO enrichment and KEGG pathway analyses on differentially expressed coding genes

All the 539 altered mRNAs underwent GO enrichment analysis and KEGG pathway analysis. The top 10 enriched GO terms on upregulated genes were listed including immune system process (ontology: biological process, GO: 0002376), extracellular region (ontology: cellular component, GO: 0005576) and binding (ontology: molecular function, GO: 0005488) (Fig. 3). On the other hand, the top 10 enriched GO term on downregulated genes were listed including sodium-independent organic anion transport (ontology: biological process, GO: 0043252), extracellular region (ontology: cellular component, GO: 0005576) and exopeptidase activity (ontology: molecular function, GO: 0008238) (Fig. 4).

Table 1. The primer sequences designed for qRT-PCR.

| Gene name	Forward and reverse primer	Product length (bp)
β-actin	F:5' GTGCTATGTTGCTCTAGACTTCG 3' R:5' ATGCCACAGGATTCCATACC 3'	174
ENSMUST00 000165968	F:5' CAGGATGCAGCAGGTGGAAGC 3' R:5' TGCTCCAGGCTGTAGTCTGTGG 3'	132
ENSMUST00 000153785	F:5' AGGTTCCTCTCCTAGCAGATCATTCTC 3' R:5' GAGCGGCAACTTCTGAGGTCTTAC 3'	99
ENSMUST00 000134409	F:5' GCTGAGTCCTCTTGCTGTGCTC 3' R:5' GTACCTGGAGGCTTGGCATGAC 3'	158
ENSMUST00 000154285	F:5' CCGCTTGGTGGTGCATGTATCC 3' R:5' CCAAGGTGCTGAGTGGCTAAGG 3'	184
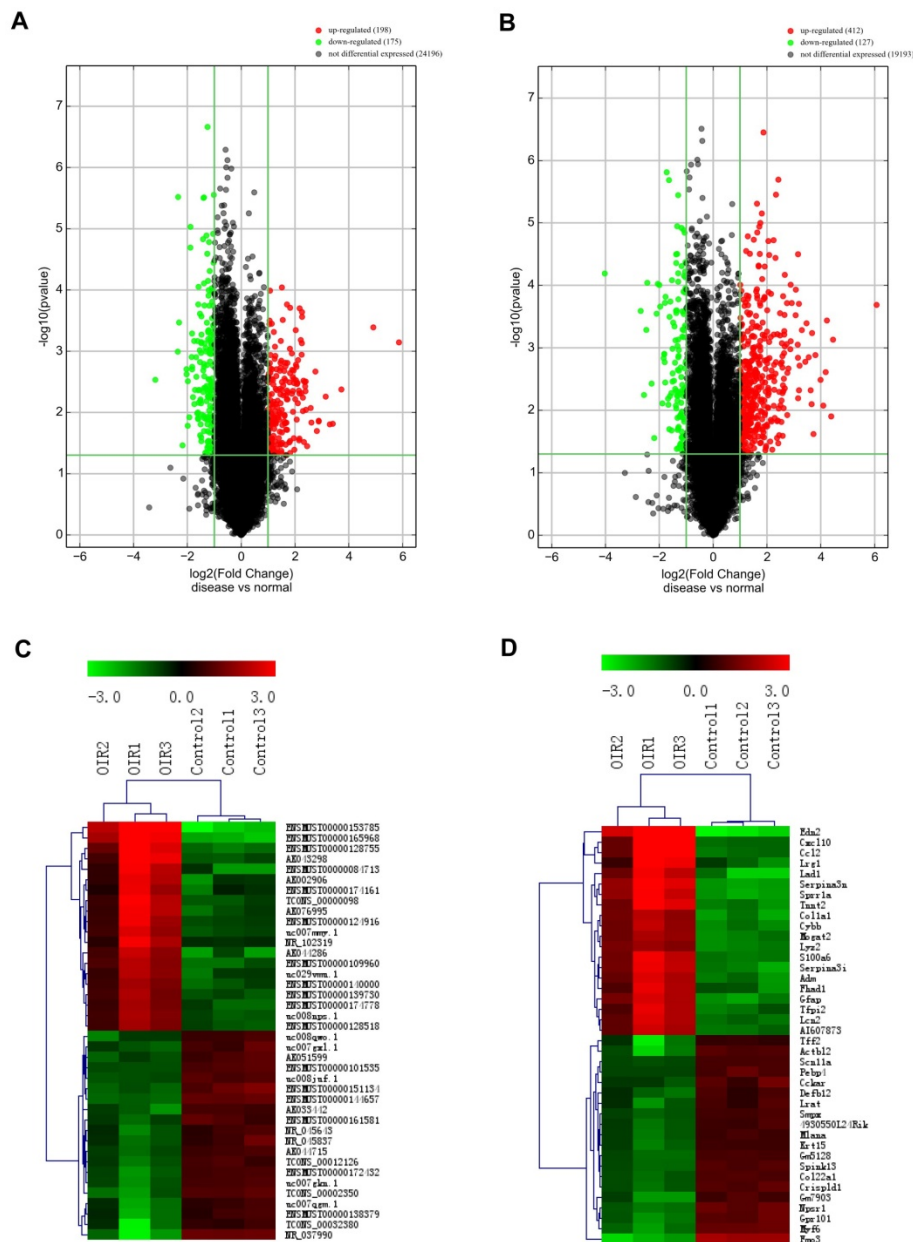
Figure 1. Both lncRNA and mRNA expression profiles were altered in the retinas of mice with oxygen-induced retinopathy (OIR) compared with control retinas. A and B, the volcano plots display the fold-changes and p-values of differential lncRNA (A) and mRNA (B) expression in OIR retinas. Based on the relationship between fold-change and statistical significance, subsets of lncRNAs and mRNAs were isolated. The vertical line corresponds to 2-fold change (up and down), respectively, and the horizontal line represents P=0.05. The red point represents the upregulated lncRNAs or mRNAs with statistical significance P < 0.05, while the green point represents the significantly decreased lncRNA or mRNA expressions. C and D, the heatmap of the top 20 differentially expressed lncRNAs (C) and mRNAs (D) in OIR groups. Each row represents the relative expression level of a lncRNA or a mRNA, and each column displays the expression level of a retina sample. Colors represent relative intensity of each sample. Red, high relative expression; green, low relative expression; black, no difference.

Table 2. Validated lncRNAs with significantly altered expression in OIR retinas with their nearby coding mRNA expression.

lncRNA Name	Nearby Gene	Relationship between lncRNA and nearby gene[a]	lncRNA expression in microarray				mRNA expression in microarray			
			Expression level	Fold change	P-value	FDR	Expression level	Fold change	P-value	FDR
ENSMUST00000165968	Serpina3j	upstream	up	30.11	0.0004	0.0349	up	3.64	0.0002	0.0178
	Serpina3i							13.93	0.0013	0.0382
	Serpina3g							2.58	0.0020	0.0460
	Serpina3n							21.95	0.0007	0.0300
ENSMUST00000153785	Fgf2	intronic antisense	up	58.30	0.0007	0.0411	up	2.25	0.0030	0.0526
ENSMUST00000134409	Col4a2	upstream	down	2.60	0.0123	0.1240	up	2.20	0.0019	0.0444
ENSMUST00000154285	C1qa	downstream	down	2.46	0.0129	0.1267	up	3.23	0.00005	0.0112

a, upstream or downstream, the genomic position of the coding gene is within 300kb upstream or downstream of the differentially expressed lncRNA region. Intronic antisense, the genomic position of the coding gene is located in the antisense strand of lncRNA intron.

Table 3. Top 20 upregulated lncRNAs identified by the microarray analysis.

SeqName	P-value	FDR	Fold Change	Regulation	Strand	Relationship	OIR 1	OIR 2	OIR 3	Control 1	Control 2	Control 3
ENSMUST00000153785	0.000717	0.041078	58.296270	up	-	intronic antisense	12.748014	10.783653	11.958061	6.109738	5.469894	6.314101
ENSMUST00000165968	0.000409	0.034852	30.109933	up	-	intergenic	8.449434	6.941674	7.838548	2.890805	2.992069	2.610279
ENSMUST00000128755	0.004214	0.079423	13.221707	up	-	exon sense-overlapping	9.614595	7.468352	8.861307	4.748751	5.034332	4.986661
AK043298	0.015278	0.137199	10.588272	up	-	intronic antisense	7.422740	4.626696	6.647810	2.720966	2.776193	2.986901
ENSMUST00000084713	0.015632	0.138298	9.804105	up	+	natural antisense	8.423589	6.038433	7.642350	3.663067	4.905065	3.656082
AK044286	0.005517	0.087954	8.824446	up	-	intergenic	6.588106	5.014738	5.853877	3.387348	2.322640	2.322215
TCONS_00000098	0.013644	0.130032	7.373443	up	+	intronic antisense	6.376250	4.062401	5.523742	2.322231	2.322640	2.670507
AK076995	0.014021	0.132143	7.371760	up	+	intergenic	13.404888	11.165535	12.681263	9.608284	9.148856	9.848519
AK002906	0.020071	0.154626	7.029474	up	-	intronic antisense	7.653271	5.450538	6.973938	4.281011	3.129105	4.227380
ENSMUST00000109960	0.002150	0.059662	6.769551	up	+	exon sense-overlapping	8.496722	7.243502	7.930245	4.976211	4.986118	5.430960
ENSMUST00000124916	0.014606	0.134809	6.111074	up	+	exon sense-overlapping	7.861429	5.677544	6.847170	4.184352	4.080745	4.286768
uc007mmy.1	0.008464	0.106702	5.992399	up	-	intergenic	7.930451	6.101834	7.092284	4.500277	4.299462	4.575429
ENSMUST00000174161	0.035534	0.197475	5.468632	up	-	exon sense-overlapping	7.971536	5.525110	6.948038	4.791939	3.697002	4.602203
uc029vmu.1	0.009057	0.109769	5.298308	up	-	intergenic	7.293197	5.804285	6.782840	4.464540	3.703680	4.495507
uc008nps.1	0.003121	0.070411	5.271589	up	-	exon sense-overlapping	7.488088	6.237517	6.975574	4.357455	4.696039	4.452972
ENSMUST00000174778	0.004496	0.080692	5.242659	up	-	intergenic	5.510269	4.239752	4.961743	2.322231	2.896421	2.322215
ENSMUST00000140000	0.003751	0.074957	5.202250	up	+	natural antisense	11.112645	9.900810	10.629968	8.155371	7.874338	8.476307
ENSMUST00000139730	0.003180	0.070468	5.121506	up	-	exon sense-overlapping	6.917978	5.666435	6.221930	4.070318	3.890004	3.776317
NR_102319	0.030389	0.184947	5.035999	up	+	intergenic	8.337279	5.907723	7.444553	4.834966	4.924242	4.933513
ENSMUST00000128518	0.003024	0.069549	4.980561	up	+	intronic antisense	11.217601	10.039138	10.746596	8.285136	8.572280	8.196994

Note: FDR: false discovery rate; Fold change: the absolute ratio (no log scale) of average normalized intensities between two groups (Control vs OIR); OIR 1-3 and Control 1-3: each sample's normalized intensity (log2 scale). Similarly hereinafter.

Table 4. Top 20 downregulated lncRNAs identified by the microarray analysis.

SeqName	P-value	FDR	Fold Change	Regulation	Strand	Relationship	OIR 1	OIR 2	OIR 3	Control 1	Control 2	Control 3
NR_037990	0.002930	0.068842	9.133963	down	-	intergenic	6.496983	8.179386	7.582079	10.578837	10.609151	10.644182
TCONS_00002350	0.001018	0.044913	5.122573	down	-	intergenic	3.398719	3.932456	4.328286	6.167787	6.210308	6.351972
ENSMUST00000144657	0.000003	0.005941	5.077183	down	-	intergenic	3.286124	3.147485	3.127405	5.459278	5.546184	5.587637
ENSMUST00000151134	0.000340	0.033792	4.954950	down	+	exon sense-overlapping	5.979015	5.713499	5.694462	8.139835	7.774910	8.398843
TCONS_00032380	0.034449	0.195020	4.527209	down	+	intergenic	2.325546	4.667767	3.856036	5.671859	5.771139	5.942216
uc007gkn.1	0.001968	0.057266	4.089872	down	-	intergenic	4.373150	5.274554	5.118756	6.920329	6.895577	7.046721
ENSMUST00000172432	0.002383	0.062812	4.076810	down	+	exon sense-overlapping	7.235149	8.230403	7.929420	9.829141	9.772890	9.875263
ENSMUST00000138379	0.016487	0.142047	3.963568	down	-	intergenic	3.852936	5.523289	4.670400	6.755349	6.409639	6.842036
AK033442	0.003089	0.070273	3.946389	down	+	intergenic	4.226163	4.571180	3.525945	6.125788	6.133114	6.005986
uc007qgm.1	0.011972	0.123334	3.800768	down	-	intergenic	3.220853	4.704746	3.926131	5.841821	5.717811	6.070972
uc008juf.1	0.000020	0.012523	3.701798	down	+	natural antisense	4.666801	4.596779	4.770185	6.444632	6.660882	6.592930
ENSMUST00000101535	0.000009	0.009977	3.691835	down	-	bidirectional	2.325546	2.384761	2.322128	4.222979	4.121313	4.341157
uc007gxl.1	0.001245	0.048164	3.582029	down	+	intergenic	2.774715	3.120723	2.579922	4.422965	4.601643	4.973084
AK051599	0.000514	0.036142	3.544961	down	-	intergenic	5.247084	4.775668	4.983758	6.846470	6.620034	7.017314
TCONS_00012126	0.001979	0.057322	3.538878	down	+	intronic antisense	2.325546	3.137978	2.842555	4.746606	4.590341	4.439007
ENSMUST00000161581	0.001803	0.055911	3.535215	down	+	intronic antisense	4.429070	5.057126	4.958622	6.669437	6.881586	6.359189
NR_045837	0.005624	0.089054	3.459985	down	+	intergenic	2.325546	3.143285	2.710571	4.403620	4.185882	4.962196
AK044715	0.000682	0.040064	3.358611	down	+	intronic antisense	5.603129	6.181402	6.033230	7.678702	7.586453	7.796200
NR_045643	0.007305	0.100085	3.344530	down	-	intron sense-overlapping	8.272287	9.375150	8.883848	10.638966	10.331851	10.785879
uc008qwo.1	0.004288	0.079723	3.282559	down	-	intronic antisense	4.425972	3.572821	4.425015	5.793922	5.771023	6.003325

Table 5. Top 20 upregulated mRNAs identified by the microarray analysis.

SeqName	Gene Symbol	P-value	Fold Change	Regulation	Chrom	OIR 1	OIR 2	OIR 3	Control 1	Control 2	Control 3
NM_007902	Edn2	0.000205	67.381397	up	chr4	11.852624	10.303807	11.289775	4.877096	5.045049	5.301226
NM_009252	Serpina3n	0.000737	21.945872	up	chr12	9.307844	7.668389	8.591409	4.155878	3.957815	4.086316
NM_021274	Cxcl10	0.012493	20.920455	up	chr5	10.216826	6.826442	9.337704	4.328950	4.440061	4.451434
NM_009264	Sprr1a	0.000364	18.752312	up	chr3	10.062212	8.794292	9.433780	5.356192	5.026828	5.220274
NM_133664	Lad1	0.002447	18.169869	up	chr1	7.659905	6.033975	7.007441	3.506036	2.322640	2.322215
NM_011333	Ccl2	0.008392	17.072770	up	chr11	10.247771	7.412768	9.424877	4.785440	4.976798	5.042302

SeqName	Gene Symbol	P-value	Fold Change	Regulation	Chrom	OIR 1	OIR 2	OIR 3	Control 1	Control 2	Control 3
NM_001130176	Tnnt2	0.003248	15.923864	up	chr1	10.822550	8.708082	10.084477	5.902835	6.098196	5.634722
NM_001199940	Serpina3i	0.001304	13.928220	up	chr12	8.721851	7.263056	8.195904	4.538610	4.381300	3.861084
NM_029796	Lrg1	0.023929	13.268675	up	chr17	8.218846	4.754638	6.925944	3.403098	2.920299	2.386174
NM_010277	Gfap	0.000579	12.789066	up	chr11	15.814435	14.657697	15.289936	11.587811	11.295535	11.848205
NM_011313	S100a6	0.001415	11.725444	up	chr3	12.736235	11.184588	12.090365	8.514794	8.378681	8.463001
NM_007742	Col1a1	0.000404	11.093194	up	chr11	7.350857	6.503708	6.813182	3.296546	3.810072	3.146321
NM_009627	Adm	0.001672	10.740590	up	chr7	9.376728	7.938694	8.770966	5.289006	5.578209	4.944169
NM_007807	Cybb	0.000520	9.827009	up	chrX	6.284053	5.254420	5.689879	2.322231	2.693649	2.322215
NM_008491	Lcn2	0.001927	9.274859	up	chr2	10.781325	9.284550	10.217709	6.831314	7.035850	6.776445
NM_009364	Tfpi2	0.004769	9.134172	up	chr6	9.771275	7.940594	9.080595	5.493661	5.638994	6.085987
NM_177448	Mogat2	0.000197	9.117081	up	chr7	7.704113	6.972424	7.414555	3.980103	4.155026	4.390246
NM_177868	Fhad1	0.006403	8.921200	up	chr4	9.166995	7.314457	8.454878	5.459930	5.392350	6.123388
NM_017372	Lyz2	0.000032	8.909107	up	chr10	9.377222	8.941198	9.078166	5.838286	5.975234	6.117223
NM_001204910	AI607873	0.001438	8.888613	up	chr1	8.415281	7.072290	7.920147	4.528947	4.592748	4.830148

Table 6. Top 20 downregulated mRNAs identified by the microarray analysis.

| SeqName	Gene Symbol	P-value	Fold Change	Regulation	Chrom	OIR 1	OIR 2	OIR 3	Control 1	Control 2	Control 3
NM_008030	Fmo3	0.000064	16.284224	down	chr1	2.825890	2.364353	3.137431	6.911447	6.719705	6.772731
NM_008657	Myf6	0.000256	6.457197	down	chr10	4.612338	5.304050	5.222832	7.700051	7.722884	7.789008
NM_175497	Actbl2	0.005672	5.932106	down	chr13	2.325546	3.940411	3.371026	5.865282	5.703255	5.774079
NM_001033360	Gpr101	0.000516	5.585098	down	chrX	5.267588	6.034113	5.634033	8.066730	7.992215	8.321536
NM_175678	Npsr1	0.000091	5.447918	down	chr9	4.373860	4.804202	4.524192	7.082227	6.838859	7.118283
ENSMUST00000113172	Gm7903	0.003727	4.876647	down	chrX	2.325546	3.421091	2.322128	4.864159	5.154450	4.907825
NM_009363	Tff2	0.027743	4.556195	down	chr17	3.511692	5.727574	4.891790	6.904248	6.953879	6.836418
NM_031402	Crispld1	0.000284	4.285419	down	chr1	5.009625	5.520657	5.393212	7.386189	7.269699	7.565915
NM_001168423	Spink13	0.000095	4.155850	down	chr18	7.918376	8.298454	7.956590	10.150014	10.016010	10.172827
NM_027174	Col22a1	0.000099	3.989103	down	chr15	6.579486	6.996267	6.898594	8.816916	8.862802	8.782823
NM_183320	Gm5128	0.000218	3.909112	down	chrX	2.325546	2.784199	2.322128	4.435049	4.475323	4.422023
NM_023624	Lrat	0.007738	3.690353	down	chr3	8.957304	10.177897	9.685661	11.532595	11.234553	11.704990
NM_008469	Krt15	0.001462	3.582905	down	chr11	6.272760	7.090776	6.681673	8.530754	8.508751	8.529093
NM_023774	4930550L24Rik	0.001266	3.519266	down	chrX	3.887049	4.602469	4.240050	5.997637	5.947053	6.230702
NM_029993	Mlana	0.001245	3.515738	down	chr19	5.456453	6.205720	5.873087	7.599213	7.764418	7.613112
NM_009827	Cckar	0.001693	3.481647	down	chr5	4.075800	4.090868	3.695177	5.778705	5.391791	6.090659
NM_025357	Smpx	0.000191	3.458745	down	chrX	2.325546	2.764756	2.542606	4.297434	4.275888	4.430330
NM_152802	Defb12	0.003577	3.430810	down	chr8	3.179997	3.787608	2.912021	5.212757	4.811799	5.190719
NM_028526	Pebp4	0.000152	3.406140	down	chr14	2.325546	2.322138	2.322128	3.930714	4.340979	4.002533
NM_011887	Scn11a	0.000002	3.304723	down	chr9	6.678956	6.791706	6.766182	8.453526	8.449595	8.507312
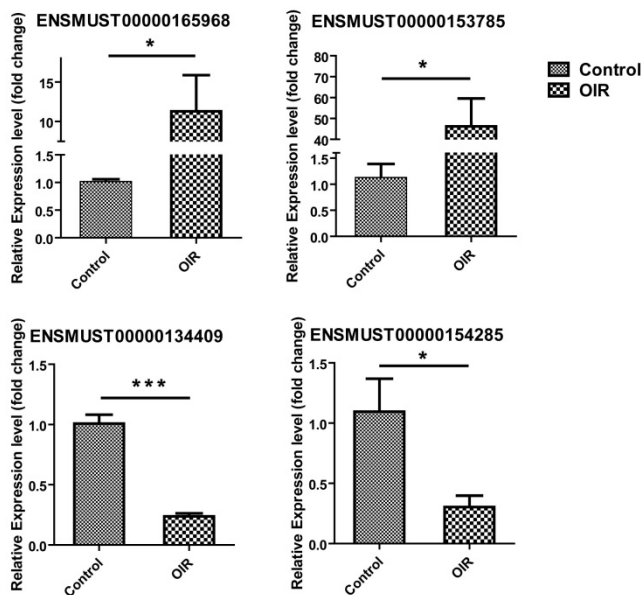
Figure 2. Validation of differential lncRNA expression by qRT-PCR. Relative expression of lncRNAs ENSMUST00000165968, ENSMUST00000153785, ENSMUST00000134409, and ENSMUST00000154285 in the retina from OIR and control mice was shown. As compared to control, n = 4 for each group. *, P < 0.05; ***, P < 0.001, *Student t*-test.

KEGG pathway analysis was conducted and demonstrated that the upregulated genes were involved in ECM-receptor interaction, phagosome, PI3K-Akt signaling pathway, and TNF signaling pathway (Fig. 5A). While downregulated genes were enriched in the pathways including protein digestion and absorption, vitamin digestion and absorption, and neuroactive ligand-receptor interaction (Fig. 5B).

The lncRNA-mRNA co-expression network with GO enrichment and KEGG pathway analyses

CNC network analysis was constructed according to 4 validated differentially expressed lncRNAs with 410 interacted mRNAs. It was composed of 414 nodes (lncRNAs and mRNAs) and 509 edges to connect these nodes, which include 280 positive (continuous lines) and 229 negative (dotted lines) interactions between lncRNAs and mRNAs (Fig. 6). Three of the selected 4 lncRNAs (ENSMUST000001659 68, ENSMUST00000153785 and ENSMUST000001344 09) were connected by mRNAs. In particular, two
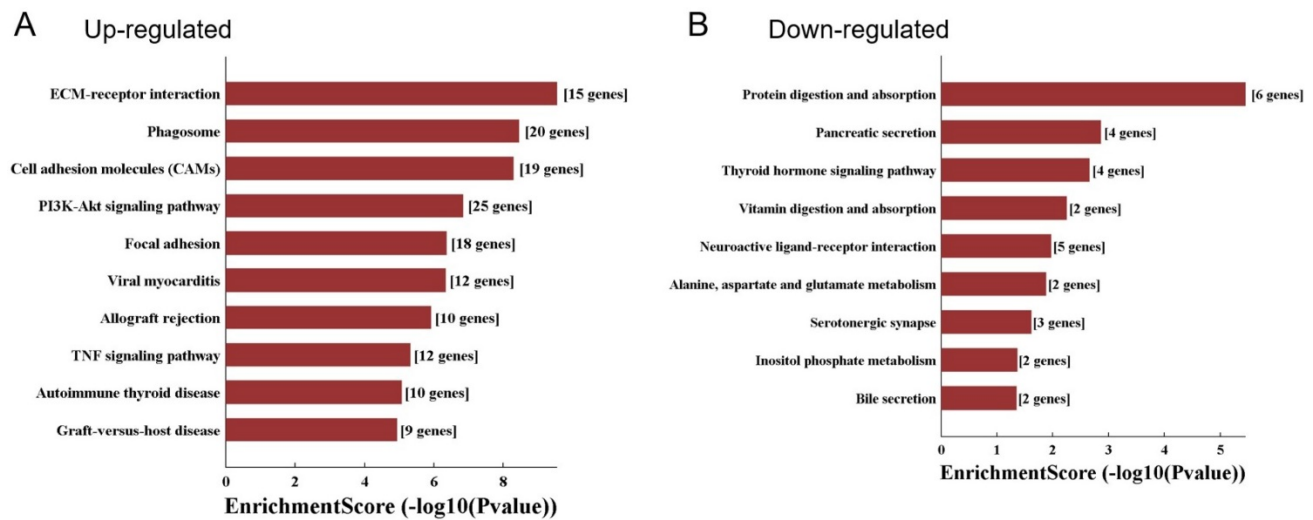
upregulated lncRNAs, ENSMUST00000165968 and ENSMUST00000153785 were connected by a large number of mRNAs, which demonstrated that these lncRNAs might have more common functional pathways in retinal neovascularization.

Figure 3. The GO analysis of significantly up-regulated mRNAs.

Figure 4. The GO analysis of significantly down-regulated mRNAs.

Figure 5. KEGG pathway analysis of differentially expressed mRNAs. A. The top 10 significant pathways which were correlated with the up-regulated genes. B. The top 9 significant pathways which were correlated with the down-regulated genes.
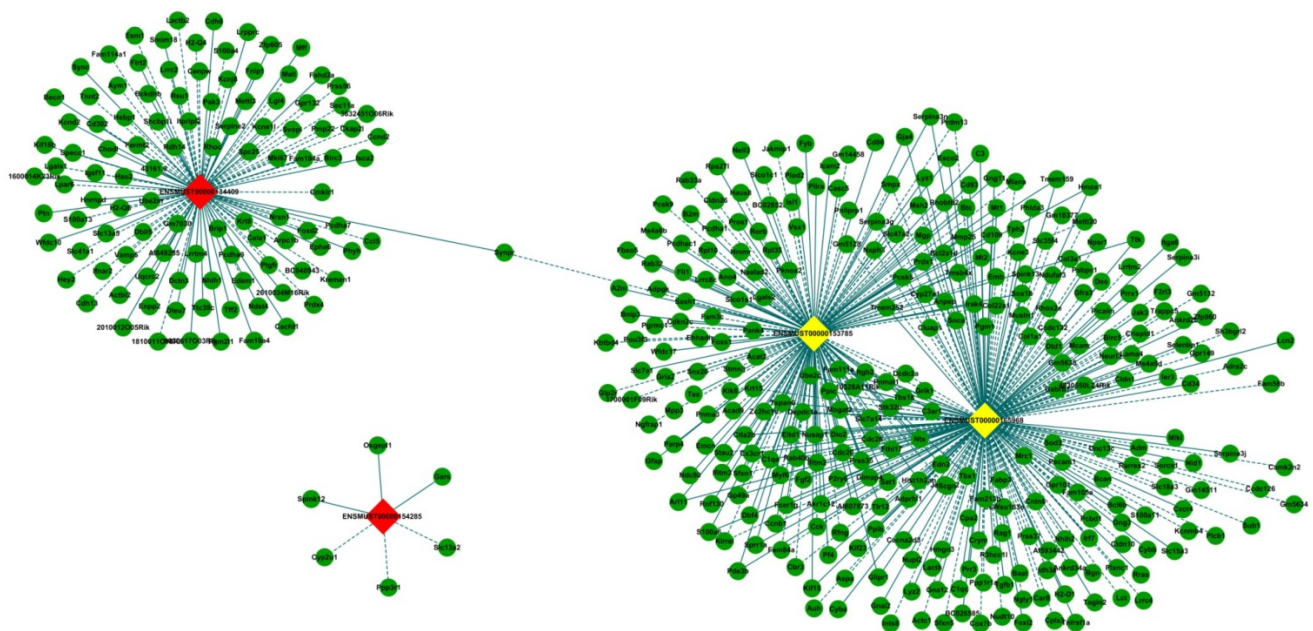
Figure 6. The lncRNA-mRNA co-expression network. LncRNAs and mRNAs with PCCs≥ 0.99 were selected to construct the network. The network shows the interaction among the lncRNAs and their potential regulated coding genes. Box nodes represent lncRNAs, and circle nodes (green) represent interacted mRNAs. Yellow represents up-regulated lncRNA, and red represents down-regulated lncRNA. Continuous edges show the positive relationship between lncRNAs and mRNAs, while dotted edges describe the inhibitive relationship.

In order to predict the functions of the lncRNAs, we performed GO and KEGG pathway analyses of those interacted mRNAs according to the results of the CNC network. The top 10 enriched GO terms on these interacted genes were listed including blood vessel development (ontology: biological process, GO: 0001568), cell part (ontology: cellular component, GO: 0044464) and binding (ontology: molecular function, GO: 0005488) (Fig. 7). On the other hand, KEGG pathway analysis showed the top 10 pathways of those interacted mRNAs enriched, including cell adhesion molecules (Fig. 8).

Discussion

Previous studies investigated the role of several kinds of molecules and cells in retinal neovascularization by OIR mouse model [24-27]. By using microarray analysis, a study assessed the lncRNA expression profiles in the retina of OIR mice; however, the study only examined lncRNA expression in OIR retinas at P7, P12 and P17, and have not compared the OIR retinas to room air controls at the same time point [28]. In the present study, we analyzed the lncRNAs and mRNAs expressions in OIR retinas compared to room air controls at the same age of P17 (the peak of

neovascularization [19]), which indicated the comparison between disease group and healthy control group.

In the present study, the altered mRNA-based GO enrichment analysis has shed light on the mechanism of retinal neovascularization in OIR. Immune system process [29, 30] and response to stress [31] are well-established factors contributing to the pathogenesis of retinal neovascularization. For example, IL-12 was reported to reduce both avascular areas and neovascular tufts in OIR mice retina through enhancing the expressions of IFN-γ and other downstream chemokines [25]. Furthermore, the over-production of reactive oxygen species (ROS) triggered by retinal hypoxia in OIR situation often activates NADPH oxidase, and in turn arouses intravitreal neovascularization by the activation JAK/STAT pathway [32, 33]. In addition, our results also implicate that some other unreported biological processes such as anion or ion transport were also involved in the retinal neovascularization of OIR mice.

Our pathway analysis on mRNAs suggested some crucial pathogenic mechanisms about retinal neovascularization. For example, a number of studies have shown that vitreous collagen and integrins [34, 35] provide essential substrates for the preretinal vasculature. This is in line with our findings that upregulated genes were also enriched in the ECM-receptor interaction pathway. Moreover, some other

pathways, such as PI3K-Akt signaling pathway [36, 37], and TNF signaling pathway [38] have been widely reported to impact the retinal neovascularization, and were also been enriched in our present study (Fig. 5A). We also mentioned some pathways regarding cellular basic processes, including protein digestion and absorption, vitamin digestion and absorption, which indicated that OIR situation would harm the metabolism of the retina.

Our microarray data suggested that several angiogenesis-related genes other than VEGF regulated by lncRNAs, such as collagen type IV alpha (COL4A)1 and COL4A2, were significantly increased in OIR mice retinas (Supplementary Table 2). Moreover, COL4A2 is a nearby gene of ENSMUST000 00134409 at upstream (Table 2). It is suggested that spontaneous retinal and subretinal neovascular lesions occurred in *COL4A1* mutant mice, and they proposed that COL4A1 or COL4A2 mutations may lead to higher risk for development of vision-threatening retinopathy [39]. Another study reported that patients with *COL4A1* mutation could develop peripheral corneal opacities with corneal neovascularization [40]. In addition, COL4A1 or COL4A2 mutations may cause ocular, cerebral, renal and muscular defects, as a result, ophthalmologic examination on retinal vascular tortuosity is recommended to evaluate COL4A1- and COL4A2-mutated cerebrovascular disease [41].
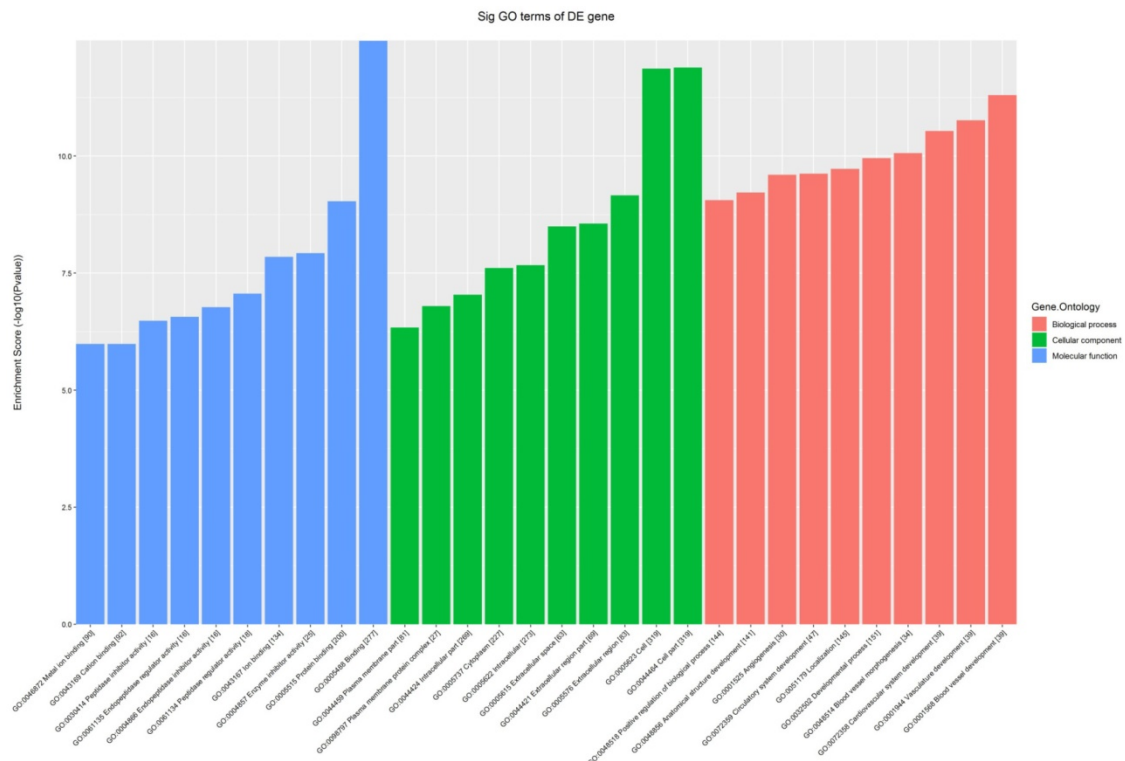

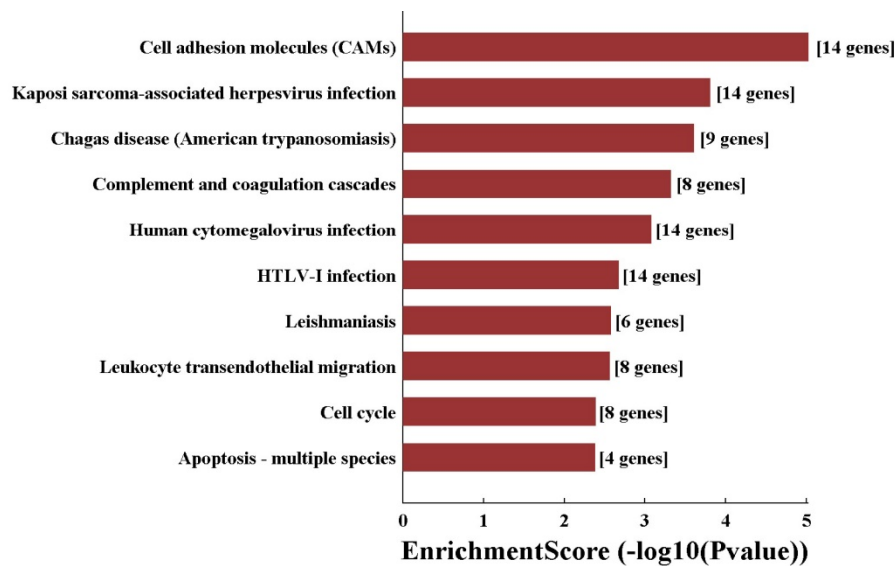**Figure 7.** The GO analysis of interacted mRNA by CNC network attributes in the target organism.

Figure 8. KEGG pathway analysis of significant pathways of interacted mRNA by CNC network.

Fibroblast growth factor (FGF) 2 is a potent pro-angiogenic factor that has been regarded as a therapeutic target in retinal neovascularization [42], and may also be important in the maintenance of neuroretinal function in OIR model [43]. In the present study, the gene of FGF2 increased to 2.25-fold (P=0.003) in OIR retinas, and act as the intronic antisense of altered lncRNA ENSMUST00000153785 (Table 2), which indicated the possible functions of lncRNA in retinal neovascular diseases. Likewise, another gene transforming growth factor-beta (TGFB) 1, which is also involved with retinal neovascularization [44, 45] was also increased significantly in OIR retinas, which is positively related with upregulated lncRNA ENSMUST00000165968 (Fig. 6).

The GO analysis of the CNC network revealed that the interacted genes regulated by altered lncRNAs are mainly involved in blood vessel development, vasculature development and angiogenesis (Fig. 8), suggesting that the altered lncRNAs play critical roles in the pathogenesis of retinal neovascularization through regulation of its target genes. Leukocytes play a mediated role in retinal vascular remodeling where leukocytes adhere to the vasculature by CD18 and remodel it by Fas ligand-mediated endothelial cell apoptosis [46]. We had previously demonstrated that M2-polarized macrophages were recruited by hypoxia in the inner layer of retinas in the OIR model [27]. Our KEGG analysis showed that the interacted genes were enriched in cell adhesion molecules (CAMs) and leukocyte transendothelial migration, indicating that leukocyte including macrophage adhesion molecules might be involved in the mechanisms of pathological retinal neovascularization through lncRNA regulation.

In conclusion, we demonstrated that numerous lncRNAs and mRNAs are significantly altered in the retina of OIR mice compared to control mice. Further, *in silico* analysis indicate that altered lncRNAs were enriched in a variety of biological process that being related to angiogenesis and vasculature development as well as cell adhesion molecules pathway. Our results highlighted that altered lncRNAs and its target genes play important roles in the ischemia-induced retinal angiogenesis however functional assessment of individual lncRNA should be guaranteed in future studies to illustrate their roles in retinal neovascularization.

Abbreviations

PDR: proliferative diabetic retinopathy; ROP: retinopathy of prematurity; lncRNA: long non-coding RNA; mRNA: messenger RNA; OIR: oxygen-induced retinopathy; GO: Gene Ontology; KEGG: Kyoto Encyclopedia of Genes and Genomes; CNC: coding-non-coding gene co-expression; VEGF: vascular endothelial growth factor; qRT-PCR: quantitative real-time reverse transcription polymerase chain reaction; PCCs: Pearson correlation coefficients; COL4A: collagen type IV alpha; FGF: fibroblast growth factor; TGFB: transforming growth factor-beta; CAMs: cell adhesion molecules.

Supplementary Material

Supplementary tables.
http://www.medsci.org/v16p0537s1.xlsx

Acknowledgements

Competing Interests

The authors have declared that no competing interest exists.

References

1. Yoshida A, Yoshida S, Ishibashi T, Inomata H. Intraocular neovascularization. Histol Histopathol. 1999; 14: 1287-94.
2. Osaadon P, Fagan XJ, Lifshitz T, Levy J. A review of anti-VEGF agents for proliferative diabetic retinopathy. Eye. 2014; 28: 510-20.
3. Stitt AW, Curtis TM, Chen M, Medina RJ, McKay GJ, Jenkins A, et al. The progress in understanding and treatment of diabetic retinopathy. Prog Retin Eye Res. 2016; 51: 156-86.
4. Salam A, Mathew R, Sivaprasad S. Treatment of proliferative diabetic retinopathy with antiVEGF agents. Acta Ophthalmol (Copenh). 2011; 89: 405-11.
5. Bohmdorfer G, Wierzbicki AT. Control of Chromatin Structure by Long Noncoding RNA. Trends Cell Biol. 2015; 25: 623-32.
6. Yang G, Lu X, Yuan L. LncRNA: a link between RNA and cancer. Biochim Biophys Acta. 2014; 1839: 1097-109.
7. Moran I, Akerman I, van de Bunt M, Xie R, Benazra M, Nammo T, et al. Human beta cell transcriptome analysis uncovers lncRNAs that are tissue-specific, dynamically regulated, and abnormally expressed in type 2 diabetes. Cell Metab. 2012; 16: 435-48.
8. Rapicavoli NA, Qu K, Zhang J, Mikhail M, Laberge RM, Chang HY. A mammalian pseudogene lncRNA at the interface of inflammation and anti-inflammatory therapeutics. Elife. 2013; 2: e00762.
9. Yang L, Lin C, Jin C, Yang JC, Tanasa B, Li W, et al. lncRNA-dependent mechanisms of androgen-receptor-regulated gene activation programs. Nature. 2013; 500: 598-602.
10. Sun X, Yuan Y, Xiao Y, Lu Q, Yang L, Chen C, et al. Long non-coding RNA, Bmcob, regulates osteoblastic differentiation of bone marrow mesenchymal stem cells. Biochem Biophys Res Commun. 2018.
11. Liu K, Yao H, Wen Y, Zhao H, Zhou N, Lei S, et al. Functional role of a long non-coding RNA LIFR-AS1/miR-29a/TNFAIP3 axis in colorectal cancer resistance to pohotodynamic therapy. Biochim Biophys Acta Mol Basis Dis. 2018; 1864: 2871-80.
12. Jia J, Zhang M, Li Q, Zhou Q, Jiang Y. Long noncoding ribonucleic acid NKILA induces the endoplasmic reticulum stress/autophagy pathway and inhibits the nuclear factor-k-gene binding pathway in rats after intracerebral hemorrhage. J Cell Physiol. 2018; 233: 8839-49.
13. Yan B, Tao ZF, Li XM, Zhang H, Yao J, Jiang Q. Aberrant expression of long noncoding RNAs in early diabetic retinopathy. Invest Ophthalmol Vis Sci. 2014; 55: 941-51.
14. Yan B, Yao J, Liu JY, Li XM, Wang XQ, Li YJ, et al. lncRNA-MIAT regulates microvascular dysfunction by functioning as a competing endogenous RNA. Circ Res. 2015; 116: 1143-56.
15. Li HB, You QS, Xu LX, Sun LX, Abdul Majid AS, Xia XB, et al. Long Non-Coding RNA-MALAT1 Mediates Retinal Ganglion Cell Apoptosis Through the PI3K/Akt Signaling Pathway in Rats with Glaucoma. Cell Physiol Biochem. 2017; 43: 2117-32.
16. Zhou RM, Wang XQ, Yao J, Shen Y, Chen SN, Yang H, et al. Identification and characterization of proliferative retinopathy-related long noncoding RNAs. Biochem Biophys Res Commun. 2015; 465: 324-30.
17. Huang J, Yang Y, Fang F, Liu K. MALAT1 modulates the autophagy of retinoblastoma cell through miR-124-mediated stx17 regulation. J Cell Biochem. 2018; 119: 3853-63.
18. Liu JY, Yao J, Li XM, Song YC, Wang XQ, Li YJ, et al. Pathogenic role of lncRNA-MALAT1 in endothelial cell dysfunction in diabetes mellitus. Cell Death Dis. 2014; 5: e1506.
19. Connor KM, Krah NM, Dennison RJ, Aderman CM, Chen J, Guerin KI, et al. Quantification of oxygen-induced retinopathy in the mouse: a model of vessel loss, vessel regrowth and pathological angiogenesis. Nat Protoc. 2009; 4: 1565-73.
20. Yamaji Y, Yoshida S, Ishikawa K, Sengoku A, Sato K, Yoshida A, et al. TEM7 (PLXDC1) in neovascular endothelial cells of fibrovascular membranes from patients with proliferative diabetic retinopathy. Invest Ophthalmol Vis Sci. 2008; 49: 3151-7.
21. Ishikawa K, Yoshida S, Nakao S, Sassa Y, Asato R, Kohno R, et al. Bone marrow-derived monocyte lineage cells recruited by MIP-1beta promote physiological revascularization in mouse model of oxygen-induced retinopathy. Lab Invest. 2012; 92: 91-101.
22. Livak KJ, Schmittgen TD. Analysis of relative gene expression data using real-time quantitative PCR and the 2(-Delta Delta C(T)) Method. Methods. 2001; 25: 402-8.
23. Engreitz JM, Haines JE, Perez EM, Munson G, Chen J, Kane M, et al. Local regulation of gene expression by lncRNA promoters, transcription and splicing. Nature. 2016; 539: 452-5.
24. Yamaguchi M, Nakao S, Arita R, Kaizu Y, Arima M, Zhou Y, et al. Vascular Normalization by ROCK Inhibitor: Therapeutic Potential of Ripasudil (K-115) Eye Drop in Retinal Angiogenesis and Hypoxia. Invest Ophthalmol Vis Sci. 2016; 57: 2264-76.
25. Zhou Y, Yoshida S, Kubo Y, Kobayashi Y, Nakama T, Yamaguchi M, et al. Interleukin-12 inhibits pathological neovascularization in mouse model of oxygen-induced retinopathy. Sci Rep. 2016; 6: 28140.
26. Nakama T, Yoshida S, Ishikawa K, Kubo Y, Kobayashi Y, Zhou Y, et al. Therapeutic Effect of Novel Single-Stranded RNAi Agent Targeting Periostin in Eyes with Retinal Neovascularization. Molecular therapy Nucleic acids. 2017; 6: 279-89.
27. Zhou Y, Yoshida S, Nakao S, Yoshimura T, Kobayashi Y, Nakama T, et al. M2 Macrophages Enhance Pathological Neovascularization in the Mouse Model of Oxygen-Induced Retinopathy. Invest Ophthalmol Vis Sci. 2015; 56: 4767-77.
28. Xu XD, Li KR, Li XM, Yao J, Qin J, Yan B. Long non-coding RNAs: new players in ocular neovascularization. Mol Biol Rep. 2014; 41: 4493-505.
29. Langer HF, Chung KJ, Orlova VV, Choi EY, Kaul S, Kruhlak MJ, et al. Complement-mediated inhibition of neovascularization reveals a point of convergence between innate immunity and angiogenesis. Blood. 2010; 116: 4395-403.
30. Zhou YD, Yoshida S, Peng YQ, Kobayashi Y, Zhang LS, Tang LS. Diverse roles of macrophages in intraocular neovascular diseases: a review. Int J Ophthalmol-Chi. 2017; 10: 1902-8.
31. Dong A, Shen J, Zeng M, Campochiaro PA. Vascular cell-adhesion molecule-1 plays a central role in the proangiogenic effects of oxidative stress. Proc Natl Acad Sci U S A. 2011; 108: 14614-9.
32. Byfield G, Budd S, Hartnett ME. The role of supplemental oxygen and JAK/STAT signaling in intravitreous neovascularization in a ROP rat model. Invest Ophthalmol Vis Sci. 2009; 50: 3360-5.
33. Hartnett ME. The effects of oxygen stresses on the development of features of severe retinopathy of prematurity: knowledge from the 50/10 OIR model. Doc Ophthalmol. 2010; 120: 25-39.
34. Bishop PN. The role of extracellular matrix in retinal vascular development and preretinal neovascularization. Exp Eye Res. 2015; 133: 30-6.
35. Campochiaro PA. Molecular targets for retinal vascular diseases. J Cell Physiol. 2007; 210: 575-81.
36. Zhuang Z, Xiao q, Hu H, Tian SY, Lu ZJ, Zhang TZ, et al. Down-regulation of microRNA-155 attenuates retinal neovascularization via the PI3K/Akt pathway. Mol Vis. 2015; 21: 1173-84.
37. You JJ, Yang CH, Yang CM, Chen MS. Cyr61 induces the expression of monocyte chemoattractant protein-1 via the integrin alphanubeta3, FAK, PI3K/Akt, and NF-kappaB pathways in retinal vascular endothelial cells. Cell Signal. 2014; 26: 133-40.
38. Mirshahi A, Hoehn R, Lorenz K, Kramann C, Baatz H. Anti-tumor necrosis factor alpha for retinal diseases: current knowledge and future concepts. J Ophthalmic Vis Res. 2012; 7: 39-44.
39. Alavi MV, Mao M, Pawlikowski BT, Kvezereli M, Duncan JL, Libby RT, et al. Col4a1 mutations cause progressive retinal neovascular defects and retinopathy. Sci Rep. 2016; 6: 18602.
40. Coupry I, Sibon I, Mortemousque B, Rouanet F, Mine M, Goizet C. Ophthalmological features associated with COL4A1 mutations. Arch Ophthalmol. 2010; 128: 483-9.
41. Kuo DS, Labelle-Dumais C, Gould DB. COL4A1 and COL4A2 mutations and disease: insights into pathogenic mechanisms and potential therapeutic targets. Hum Mol Genet. 2012; 21: R97-110.
42. Li D, Xie K, Zhang L, Yao X, Li H, Xu Q, et al. Dual blockade of vascular endothelial growth factor (VEGF) and basic fibroblast growth factor (FGF-2) exhibits potent anti-angiogenic effects. Cancer Lett. 2016; 377: 164-73.
43. Fang L, Barber AJ, Shenberger JS. Regulation of fibroblast growth factor 2 expression in oxygen-induced retinopathy. Invest Ophthalmol Vis Sci. 2014; 56: 207-15.
44. Shih SC, Ju M, Liu N, Mo JR, Ney JJ, Smith LE. Transforming growth factor beta1 induction of vascular endothelial growth factor receptor 1: mechanism of pericyte-induced vascular survival in vivo. Proc Natl Acad Sci U S A. 2003; 100: 15859-64.
45. Yingchuan F, Chuntao L, Hui C, Jianbin H. Increased expression of TGF-beta1 and Smad 4 on oxygen-induced retinopathy in neonatal mice. Adv Exp Med Biol. 2010; 664: 71-7.
46. Ishida S, Yamashiro K, Usui T, Kaji Y, Ogura Y, Hida T, et al. Leukocytes mediate retinal vascular remodeling during development and vaso-obliteration in disease. Nat Med. 2003; 9: 781-8.